Classical trajectory calculations for collision-energy/electron-energy resolved two-dimensional Penning ionization electron spectra of N2, CO, and CH3CN with metastable He*(2 3S) atoms

doi: 10.1063/1.1503312

Classical trajectory calculations for collision-energy/electron-energy resolved two-dimensional Penning ionization electron spectra of N_2, CO, and CH_3CN with metastable $He^*(2\,^3S)$ atoms

Masakazu Yamazaki, Satoshi Maeda, Naoki Kishimoto, and Koichi Ohno[a)]
Department of Chemistry, Graduate School of Science, Tohoku University, Aramaki, Aoba-ku, Sendai 980-8578, Japan

(Received 28 May 2002; accepted 9 July 2002)

Collision-energy/electron-energy resolved two-dimensional Penning ionization electron spectra (2D-PIES) of N_2, CO, and CH_3CN with metastable $He^*(2\,^3S)$ atoms are measured, and classical trajectory calculations with anisotropic entrance and exit potential energy surfaces are performed for these systems. Numerical qualities of the entrance potential surfaces are decisively important to understand the collisional ionization dynamics as well as to reproduce observed 2D-PIES, whereas the exit potential surfaces are less sensitive to the collisional ionization dynamics and the electron spectra except for special cases in which a deep potential well is relevant in the entrance potential surface. *Ab initio* calculations of both entrance and exit potentials as well as ionization widths are found to be reliable in obtaining their anisotropy and radial dependence with good quantitative accuracy. © *2002 American Institute of Physics.* [DOI: 10.1063/1.1503312]

I. INTRODUCTION

One of the most fundamental problems in chemical physics is to understand how chemical reactions take place. That is, how reactant particles make their journey to products. In order to elucidate chemical reaction dynamics, it is important to study details of time evolution: how particles behave from initial states to final states. In addition to such state-to-state dynamics, spatial characteristics of elementary reaction processes are of great importance for collisional reactions involving anisotropic particles. Reaction probabilities in a single-collision condition are decisively sensitive to relative geometries of reactant particles. Thus, stereo dynamics in collisional reactions should be studied in detail by theory and experiments.

One of the simplest reaction processes including collisions is a chemi-ionization process known as Penning ionization ($A^* + M \rightarrow A + M_i^+ + e^-$);[1] a molecule M collides with an excited atom A* [such as a metastable $He^*(2\,^3S)$ atom] having an excitation energy larger than the lowest ionization potential (IP) of the molecule, and then M is ionized into an ionic state of M_i^+ to eject an electron e^-. The kinetic energy of the electron (E_e) ejected in the ionization process depends on the respective ionization potential $(IP)_i$ producing the corresponding ionic state of M_i^+. If several electronic states of M_i^+ can be produced, the total ionization cross section σ_T is the sum of the partial ionization cross sections $\sigma^{(i)}$. Although σ_T can be observed by detecting produced ions, $\sigma^{(i)}$ should be measured by a sophisticated technique analyzing produced ionic states. An application of electron spectroscopic techniques to Penning ionization[2–4] has made it possible to observe partial ionization cross sections as band intensities in a Penning ionization electron spectrum (PIES).[2] Branching ratios for production of various ionic states of the molecule M_i^+ can thus be estimated from relative band intensities of PIES. Based on the electron exchange model proposed by Hotop and Niehaus,[5] ionization into a particular final ionic state should take place with a high probability when the $1s$ orbital of the He atom overlaps effectively with the target molecular orbital from which an electron is removed. Branching ratios estimated from relative band intensities of PIES can be well described with electron densities outside the repulsive surface of the molecule (exterior electron density; EED).[6–8] The exterior electron model for Penning ionization has been used to understand reactivity of molecular orbitals of various molecules in connection with the anisotropy of orbital functions as well as their stereo chemical environments.[8] Sensitivity of Penning ionization to the exterior electron distribution has been compared with electron momentum spectroscopic studies.[9,10]

Another important variable of collisional ionization is the collision energy (E_c) between A* and M,[2–4,11] because ionization cross sections are in general functions of the relative kinetic energies between the colliding particles. Although the collision energy dependence of total ionization cross sections has been studied extensively by detecting produced ions or quenching rates of metastable atoms,[12–18] collision energy dependence of ''partial'' Penning ionization cross sections (CEDPICS) has eluded observation for a long time. CEDPICSs for molecular targets were first observed by using an electron spectroscopic technique combined with time-of-flight selections of velocities of metastable atoms.[19–21] Recently, we have developed a collision-energy/electron-energy resolved two-dimensional Penning ionization electron spectroscopic (2D-PIES) technique,[22] in which the produced electron intensity is observed as a function of both E_c and E_e. This 2D-PIES technique also enables us to

a)Author to whom correspondence should be addressed. Electronic mail: ohnok@qpcrkk.chem.tohoku.ac.jp

observe collision-energy resolved Penning ionization electron spectra (CERPIES).[23] Although collision energies were selected stepwise, CERPIES were also measured for $He^*(2\,^1S)+N_2$[11,24,25] and $He^*(2\,^{1,3}S)+Ar$[11,26] by means of crossed supersonic beams.

Fundamental theories of Penning ionization for an atomic target were established by Nakamura[27] and Miller.[28] These theories require the ionization width Γ or the ionization transition rate W as well as the interaction potentials of collisional ionization processes for both the entrance (V^*) and the exit (V^+) channels. Applications of these theories to simple atomic targets such as H and Li atoms have been performed in a straightforward way; collision energy dependence of Penning ionization cross sections for atomic targets have been calculated by using *ab initio* potentials and *ab initio* ionization widths combined with a classical trajectory theory[29,30] or a quantum-mechanical scattering theory.[31,32] Numerical calculations of CERPIES have also been performed for $He^*(2\,^3S)+H$[29,30,32] and $He^*(2\,^3S)+Li$[31,33] using *ab initio* potentials and *ab initio* ionization width. Some semiempirical treatments for the ionization width were employed for He^*+He^*[34] and $He^*(2\,^3S)+H$, Li, Na.[35] Moreover, semiempirical functions were used for both potentials and width for $He^*(2\,^{1,3}S)+Ar$.[22,26,36] Recently, Ishida and Katagiri[37] did *ab initio* molecular orbital studies for $He^*(2\,^{1,3}S)+Ar$, and showed that *ab initio* ionization widths for both singlet and triplet He* deviate from the single exponential form commonly used in many studies.

In order to perform numerical calculations of CEDPICS and CERPIES for molecular target systems, anisotropic parts of potential functions and ionization width should be determined precisely. Appropriate estimation of anisotropy has been a major obstacle except for a very simple system of $He^*(2\,^{1,3}S)+H_2$ for which *ab initio* calculations and quantum scattering treatments have been made by Cohen and Lane.[38] Dunlavy *et al.* have performed quantum scattering calculations for CERPIES for $He^*(2\,^1S)+N_2$ by using semiempirical potential functions and ionization width combined with Legendre expansions.[25] Ishida and Horime have made *ab initio* calculations of CEDPICS for $He^*(2\,^3S)+N_2$.[39–41] Ogawa *et al.* have performed considerably simplified calculations including *ab initio* model potentials and ionization width to yield satisfactory agreement with observed CEDPICS for $He^*(2\,^3S)+N_2$[42] and $He^*(2\,^3S)+CH_3CN$.[43] Based on the *ab initio* models, observed 2D-PIES including both CEDPICS and CERPIES have been compared with calculations for $He^*(2\,^3S)+N_2$[44] and for $He^*(2\,^3S)+CO$.[45]

Since the entrance potential V^* is embedded among ionization continua, *ab initio* calculations of V^* for molecular targets are hardly done except for $He^*(2\,^{1,3}S)+H_2$,[38] $He^*(2\,^3S)+N_2$,[39] and $He^*(2\,^3S)+H_2O$;[46,47] *ab initio* potential curves were obtained by the Feshbach projection operator method.[48,49] An alternative approach avoiding the difficulty associated with the very high excitation energy of the superexcited state is a replacement of the metastable rare gas atom with the corresponding alkali atom on the basis of the well-known resemblance in interaction with various atomic targets;[50–53] because of the outstanding importance of the outer electron, the velocity dependence of the total scattering cross section of $He^*(2\,^3S)$ by He, Ar, and Kr is very similar to that of $Li(2\,^2S)$,[50] and the location of the potential well and its depth are very similar for both $He^*(2\,^3S)$ and $Li(2\,^2S)$ with various atomic targets.[51,52] Therefore, in place of $He^*(2\,^3S)$ a ground-state Li atom has been used in calculations of *ab initio* model potentials for V^*.[42–45] Anisotropic interaction potentials between a Li atom and molecules have been studied in many other fields; charge transfer and van der Waals interactions for CH_3CN+Li has been studied in connection with matrix ESR studies[54] and gas phase cluster studies.[55] Directions of the attractive potential wells have been discussed for CH_3Cl+He^*,[56] Ne^*,[57] and $CHCl_3+Ar^*$.[58] Recently, *ab initio* Li model potentials have been improved for N_2+He^* and $CO+He^*$.[59]

As for exit potentials V^+ between molecular ion and a ground-state He atom, *ab initio* calculations for N_2^++He[60] were applied to Penning ionization system of $He^*(2\,^1S)+N_2$.[25] Various levels of calculations for V^+ of $He^*(2\,^3S)+N_2$ have been compared in detail for theoretical reproduction of 2D-PIES;[44] almost no substantial difference of interaction potentials was found between the outer valence Green's function method (OVGF)[61] and the multireference single and double excitation configuration interaction method (MRSDCI), and even Koopmans' approximation using Hartree–Fock orbital energies gave satisfactory interaction potentials in good agreement with the observed 2D-PIES.[44] This indicates that *ab initio* calculations of interaction potential functions are much more difficult for the entrance channel rather than for the exit channel.

Although many studies employed the single exponential form for the ionization width Γ in combination with the Legendre expansion for its angular part, this may not be suitable for the following reasons: (1) As suggested by Ishida and Katagiri,[37] its radial dependence is not necessarily a single exponential, and (2) the Legendre expansion cannot be fitted easily for highly anisotropic systems. In order to take the radial and angular characteristics of Γ into account in the more realistic levels of approximation, *ab initio* calculation using molecular wave functions should be made for the ionization width.

In this study, theoretical construction of 2D-PIES based on *ab initio* calculations were made for $N_2+He^*(2\,^3S)$, $CO+He^*(2\,^3S)$, and $CH_3CN+He^*(2\,^3S)$ as typical systems, and results were compared with observed 2D-PIES. Optical potentials in the collisional reaction process, real parts of the entrance potential V^* together with the imaginary part of the ionization width Γ, as well as the exit potential V^+ were discussed in connection with their significance in the stereo reaction dynamics.

II. EXPERIMENT SECTION

The experimental apparatus used in the present study has been reported in previous papers.[19–23] A metastable beam of He was produced by a nozzle discharge source, and the $He^*(2\,^1S)$ component was quenched by a water-cooled helium discharge lamp. The metastable $He^*(2\,^3S)$ beam was pulsed by a mechanical chopper and then introduced into a

collision cell located 504 mm downstream from the chopper disk. The kinetic energy of electrons ejected with Penning ionization was measured by a hemispherical electrostatic deflection-type analyzer using an electron collection angle 90° to the incident $He^*(2\,^3S)$ beam. The transmission efficiency curve of the electron energy analyzer was determined by comparing our He I UPS data with those of Gardner and Samson[62] and Kimura *et al.*[63] The energy resolution of the electron energy analyzer was 70 meV in the measurements of N_2 and CO to obtain the vibrational structures and 200 meV for CH_3CN estimated from the full width at half maximum (fwhm) of the $Ar^+(^2P_{3/2})$ peak in the He I UPS. The background pressure in the reaction chamber was on the order of 10^{-7} Torr, and the experiments were performed under a sample pressure of ca. 2×10^{-5} Torr.

The He^* velocity distribution $I_{He^*}(\nu_{He^*})$ was obtained by measuring a time-of-flight (TOF) of electrons emitted from a stainless-steel plate inserted into the collision cell, since TOFs of secondary electrons from the metal surface to the detector are negligibly short in comparison with that of the He^* atoms. The 2D Penning ionization electron intensity of sample molecules $I_e(E_e,t)$ as functions of electron kinetic energy E_e and time t was converted to $I_e(E_e,\tau_{TOF})$ as functions of E_e and TOF of the He^* beam. The $I_e(E_e,\tau_{TOF})$ can lead to $I_e(E_e,\nu_{He^*})$ as functions of E_e and velocity of He^* atoms ν_{He^*}. By the following equations, the 2D Penning ionization cross section $\sigma(E_e,\nu_r)$ was obtained:

$$\sigma(E_e,\nu_r)=c\,\frac{I_e(E_e,\nu_{He^*})}{I_{He^*}(\nu_{He^*})}\,\frac{\nu_{He^*}}{\nu_r} \tag{1}$$

$$\nu_r=\sqrt{\nu_{He^*}^2+\frac{3k_BT}{m}} \tag{2}$$

where c is a constant, ν_r is the relative velocity averaged over the velocity of the target molecule, k_B is the Boltzmann constant, and T and m are the gas temperature and the mass of the target molecule, respectively. The cross section in Eq. (1) is normalized with the velocity distribution $I_{He^*}(\nu_{He^*})$ of He^* beam. Finally, $\sigma(E_e,\nu_r)$ is converted to $\sigma(E_e,E_c)$ by the relation

$$E_c=\tfrac{1}{2}\mu\nu_r^2 \tag{3}$$

where μ is the reduced mass of the colliding system.

III. CALCULATIONS

The most important theoretical quantities of Penning ionization are the following functions: the interaction potential V^* for the entrance channel (A^*+M), the interaction potential V_i^+ for the exit channel $(A+M_i^+)$, and the ionization width $\Gamma^{(i)}$ for the electronic transition causing ionization of the molecule into the ith ionic state associated with the deexcitation of the metastable atom to the ground state. When these functions are given, various aspects of Penning ionization can be calculated with appropriate descriptions of collision dynamics.

A. Entrance potential energy surface

In order to avoid difficulties associated with highly excited electronic states embedded in ionization continua, a Li model potential V_0 for the system of $M+Li(2\,^2S)$ was calculated in place of the entrance interaction potential V^* for $M+He^*(2\,^3S)$ on the basis of the well-known resemblance between $He^*(2\,^3S)$ and $Li(2\,^2S)$.[50–53] The Li model potential V_0 was obtained from the following equation:

$$V_0=E_{MLi}-(E_M+E_{Li}), \tag{4}$$

where E_{MLi}, E_M, and E_{Li} are the total energy of the interacting system (M+Li), the isolated molecule (M), and the isolated Li atom, respectively.

Li model potentials V_0 were calculated for N_2+Li, $CO+Li$, and CH_3CN+Li systems instead of N_2+He^*, $CO+He^*$, and CH_3CN+He^*. The GAUSSIAN program[64] was used with the following optional treatments: For N_2+Li and $CO+Li$ the coupled cluster method including single, double, and optional triple excitation CCSD(T) with 6-311+G* basis sets were used, and for CH_3CN+Li the second-order Møller–Plesset perturbation theory was used to include electron correlation effects with the basis set of 6-31++G**. Full counterpoise method[65] was employed to correct the basis-set superposition error. Molecular structures were fixed at experimental equilibrium geometries. This treatment means that intramolecular nucleus motions are negligibly slow in comparison with the motion of the He atom colliding with the target molecule. Although the experimental condition of the collision energy range (ca. 70–400 meV) is in a marginal region, this frozen molecular structure approximation has been found to be reasonable in the previous studies for $He^*(2\,^3S)+N_2$, $He^*(2\,^3S)+CO$, and $He^*(2\,^3S)+CH_3CN$.[42–45,59] Such a vibrationally adiabatic treatment has also been employed for $He^*(2\,^1S)+N_2$ by Dunlavy and Siska.[25]

In the cases of N_2+Li and $CO+Li$, the potential energy surfaces $V_0(R,\theta)$ were obtained as functions of R and θ, where R is the distance between the Li(He*) atom and the center of mass of the molecule (X), θ is the polar angle from the molecular axis. Interaction potential energies were calculated at 145 points for different orientation of N_2 with respect to Li(He*) and 186 points for $CO+Li(He^*)$. In the case of CH_3CN+Li, the potential energy surface $V_0(R,\theta,\phi)$ was obtained as functions of R, θ, and ϕ, where θ is the polar angle from the CCN axis of CH_3CN, and ϕ is the azimuthal angle. Interaction potential energies were calculated at 580 points for different orientation of CH_3CN with respect to Li(He*). Potential data were interpolated with cubic spline functions to obtain the potential energy at arbitrary orientation of the He atom and a molecule. In order to obtain the maximum efficiency to reduce essential data points, as well as to minimize inaccuracies associated with interpolations, the following procedures were employed. (1) At first, spline treatments were taken along radial directions from the center of mass of the molecule, since the asymptotic properties at the shorter and the longer distances are well-known. (2) In the second step, spline treatments were made for circular directions along with circles of suitable radii for which potential values at crossing points with radial axes could easily be obtained from the splined data determined in the first step. (3) Potential values at arbitrary points were obtained from the splined data in the first two steps at any instance of tra-

jectory calculations; a radial spline along a direction including the sampled point was performed by using already determined circular splines for various radii to yield the potential value of the sampled point very efficiently.

In the case of N_2 and CO, the lower energy parts of repulsive potential walls in the entrance potentials were found to be especially important to reproduce CEDPICS and CERPIES; therefore, a linear scaling method has been used in the previous studies:[42,44,45]

$$V_0^{\text{scaled}}(R,\theta)=aV_0(R,\theta), \tag{5}$$

where a is a scaling constant. Recently, the more flexible treatment using exponential corrections (EC) has been proposed for improving the *ab initio* Li model potentials.[59] In the present study, the EC model was used for N_2+He^* and $CO+He^*$. In the EC model, the following potential V_{EC} is introduced:

$$V_{EC}(R,\theta)=V_0(R,\theta)-\sum_i A_iP_i(\cos\theta)\exp(-R/B). \tag{6}$$

Here, R is the distance between the He*(Li) atom and the center-of-mass of the molecule, θ denotes the angle of the vector **R** directing to the He*(Li) atom from the center of mass with respect to the molecular axis, $P_i(\cos\theta)$ is the ith-order term of Legendre polynomials, and A_i and B are parameters to be optimized. For N_2+He^* and $CO+He^*$, optimized model potentials of $V_{EC}(R,\theta)$ were used as the entrance potentials V^*.

In the case of CH_3CN, the nature of the entrance potential is decisively governed by the deep potential well of ca. 380 meV around the CN group.[43] As for nitrogen or oxygen containing molecules having a deep potential well with a He* atom, Li model potentials have been found to be satisfactory in connection with observed peak shifts with respect to the corresponding photoelectron bands.[66–72] Since the modification technique of V_{EC} requires a very high computational cost, especially for highly anisotropic systems, the Li model potential V_0 was employed as V^* for CH_3CN+He^* in the present study.

B. Ionization widths

The ionization width $\Gamma^{(i)}$ of the entrance potential for producing the ith ionic state is given by

$$\Gamma^{(i)}=2\pi\rho^{(i)}|\langle\Phi_0|H_{\text{el}}|\Phi^{(i)}\rangle|^2, \tag{7}$$

where $\rho^{(i)}$ is the density of final states, H_{el} is the electronic Hamiltonian, and Φ_0 and $\Phi^{(i)}$ are the electronic wave function for the initial and final states, respectively. By using Slater determinant wave functions composed of one-electron orbitals for both initial and final states, the integral in Eq. (7) can be approximated as

$$\langle\Phi_0|H_{\text{el}}|\Phi^{(i)}\rangle\approx\langle\psi_{2s}(1)\phi_i(2)|\frac{1}{r_{12}}|\psi_{1s}(1)\phi_{\epsilon^{(i)}}(2)\rangle - \langle\psi_{2s}(1)\phi_i(2)|\frac{1}{r_{12}}|\psi_{1s}(2)\phi_{\epsilon^{(i)}}(1)\rangle, \tag{8}$$

where ψ_{2s} and ϕ_i are the $2s$ orbital of He* in the initial state and the ith orbital of the target molecule, respectively, and ψ_{1s} and $\phi_{\epsilon^{(i)}}$ are the He $1s$ orbital in the final state and the ejected electron orbital in the continuum, respectively. In case of $He^*(2\,^3S)$, the first term vanishes because of the spin inversion. The remaining second term in Eq. (8) can be approximated as a product of two overlap integrals

$$-C\langle\phi_i|\psi_{1s}\rangle\langle\psi_{2s}|\phi_{\epsilon^{(i)}}\rangle, \tag{9}$$

where C is a constant factor obtained by replacing r_{12} to an average value.[73] This overlap approximation in Eq. (9) is based on the Mulliken approximation for the two electron integral $\langle pr|qs\rangle$[74]

$$\langle pr|qs\rangle=(1/4)\langle p|q\rangle\langle r|s\rangle\{\langle pp|rr\rangle + \langle pp|ss\rangle+\langle qq|rr\rangle+\langle qq|ss\rangle\}. \tag{10}$$

This approximation has been widely used in semiempirical molecular orbital theories as well as in semiempirical treatments for electron transfer rates in various electron transport phenomena including charge transfer[75] and exciton diffusion.[76] Since the $2s$ and continuum orbitals are very diffuse, anisotropy of the ionization width is mainly governed by the compact He $1s$ and ionized molecular orbitals. Thus, the following formula can be used as the ionization width for the purpose of the present study:

$$\Gamma^{(i)}=K^{(i)}|\langle\phi_i|\psi_{1s}\rangle|^2, \tag{11}$$

where $K^{(i)}$ is a constant value for each ionic state that is determined in order to reproduce observed ionization branching ratios and collision-energy dependence. Orbital functions ϕ_i and ψ_{1s} were obtained from *ab initio* self-consistent field (SCF) calculation for the neutral molecule and a He atom with the same basis set as used in the potential calculations. It should be noted here that both ϕ_i and ψ_{1s} are orbital functions for the ground states, since the molecule in the initial state and the He atom in the final state are in their ground electronic states. It should also be noted that if the overlap integral in Eq. (11) is replaced by a single exponential function of the distance R, then the expression for the ionization width $\Gamma^{(i)}$ will become the commonly used semiempirical formula.[77,78] In the present study, in order to consider anisotropic properties as well as distortion of the radial dependence from the single exponential form, the overlap approximation of Eq. (11) was employed.

C. Classical trajectory calculations

In this study, the dynamics of Penning ionization was described within a classical treatment[42] in order to obtain CEDPICS and CERPIES. The molecular structure was fixed, and the relative motion between the center of mass of the molecule and the He* atom was determined by the equations of motion. Initial rotational energies of the molecule were generated so as to fit with the Boltzmann distribution at 300 K, and the impact parameter b was set randomly from 0 to 7 Å for N_2+He^* and $CO+He^*$ and from 0 to 9 Å for CH_3CN+He^*. The rotational motion of the molecule was treated in terms of the quaternion parameters using Euler angles.[79,80] Once a set of the initial parameters of a trajectory

was determined, then time evolution of these parameters was calculated to obtain the trajectory. For a particular initial collision energy, 3000 trajectories (10 000 for CH_3CN+He^*) were calculated with various initial parameters randomly generated.

In each trajectory step, a partial transition probability $P^{(i)}$ in a time interval dt was expressed as follows:

$$P^{(i)}(t)dt = S(t)W^{(i)}(\mathbf{R}(t))dt, \tag{12}$$

$$W^{(i)}(\mathbf{R}) = \frac{\Gamma^{(i)}(\mathbf{R})}{\hbar}, \tag{13}$$

$$S(t) = 1 - \sum_i P^{(i)}_{\text{int}}(t), \tag{14}$$

$$P^{(i)}_{\text{int}}(t) = \int_0^t P^{(i)}(t)dt, \tag{15}$$

where $W^{(i)}$ is the transition rate to the ith ionic state and $\mathbf{R}$ is the relative position of He* with respect to the molecule, which is specified by R, θ, and ϕ. $S(t)$ is a statistical survival factor for the metastable He* atom at a particular time t. This factor can be considered as the survival probability of He* in the excited state as a function of time t (or a function of the geometrical position along the trajectory). Although in a real trajectory the ionization event occurs at most once at a certain position on that trajectory, one may treat a bundle of the same trajectories in a statistical way for computational efficiency. Thus, the integrated partial ionization probability $P^{(i)}_{\text{int}}(t)$ is also a function of time (or positions), which can be determined by integration of partial ionization probability $P^{(i)}(t)$ before time t (or before arriving at the position). Then, the survival factor $S(t)$ can be obtained from the summation of $P^{(i)}_{\text{int}}(t)$ over the possible ionic states. The transition rate to the ith ionic state $W^{(i)}$ can be evaluated with the ionization widths $\Gamma^{(i)}$ at each geometrical configurations of He* and a molecule.

The partial ionization cross section $\sigma^{(i)}$ was obtained from ionization probability $P^{(i)} = P^{(i)}_{\text{int}}(\infty)$ during the whole span of the trajectory with a weight factor of $2\pi b\, db$:

$$\sigma^{(i)} = \int_0^\infty 2\pi b P^{(i)} db. \tag{16}$$

Here, b is the impact parameter. Since the initial conditions for the molecular orientation and the direction of the angular momentum vector are randomly generated to yield an isotropic treatment, each trajectory with a particular impact parameter can be treated with an equal weight to lead to the integration of Eq. (16). Theoretical CEDPICS were obtained from partial ionization cross sections $\sigma^{(i)}$ for various collision energies.

D. Exit potential energy surfaces and 2D-PIES

In order to obtain theoretical CERPIES, the kinetic energy of the ejected electron at each trajectory step should be calculated as the potential energy difference between the entrance and exit channels.[3] This relationship among the ejected electron energy and the entrance and exit potential surfaces is based on the commonly used assumption that the kinetic energy of the relative motion between the reacting particles is conserved on a vertical transition in the adiabatic approximation.

The exit potential surfaces were calculated for three ionic states of $N_2^+ + He$ and $CO^+ + He$ and for four states of $CH_3CN^+ + He$. Each exit potential surface was obtained from the vertical ionization potential (IP) for $N_2 + He$, $CO + He$, and $CH_3CN + He$ in their neutral ground states. The procedures for obtaining multiexit potential surfaces are as follows. The interaction energy $V_G(R,\theta,\phi)$ of the neutral ground state was calculated, and then the vertical IP $[\text{IP}^{(i)}(R,\theta,\phi)]$ for the ith ionic states as functions of the distance R, the angle θ, and ϕ was added to the $V_G(R,\theta,\phi)$. The exit potential energy surface $V^+_{(i)}(R,\theta,\phi)$ with the ith ionic state was thus obtained by the following equation:

$$V^+_{(i)}(R,\theta,\phi) = V_G(R,\theta,\phi) + \text{IP}^{(i)}(R,\theta,\phi) - \text{IP}^{(i)}(\infty), \tag{17}$$

where $\text{IP}^{(i)}(\infty)$ is IP of each molecule at the infinite distance between the He atom and the respective molecule. The outer valence Green's function (OVGF) method[61] was used for calculating the IPs. The relative energies of exit channels $E^+_{(i)}(R,\theta,\phi)$ to the ground state were obtained by corrections with observed IPs,[63] $\text{IP}^{(i)}_{\text{obs}}(\infty)$, of each molecule at the infinite distance between the He atom and the respective molecule

$$E^+_{(i)}(R,\theta,\phi) = \text{IP}^{(i)}_{\text{obs}}(\infty) + V^+_{(i)}(R,\theta,\phi). \tag{18}$$

Although calculated IPs by OVGF method for isolated molecules are in good agreement with the observed values within a difference of 30 meV, these discrepancies may also contribute to the total discrepancies in the theoretical 2D-PIES (or CERPIES). Since our purpose is to discuss collisional ionization dynamics and to understand the reaction processes in connection with interaction potentials and ionization widths, the IPs for the infinite distance were taken from the observed photoelectron data rather than the calculations.

The structure of the molecular cation was fixed at the structure of the neutral form, since the electronic transition can be described as a vertical transition in the collisional ionization. The electron kinetic energy $E^{(i)}_e(R,\theta,\phi)$ at an arbitrary orientation of a molecule with respect to the He atom can be calculated by

$$E^{(i)}_e(R,\theta,\phi) = E_0(R,\theta,\phi) - E^+_{(i)}(R,\theta,\phi), \tag{19}$$

where the relative energy of the entrance channel to the ground state is denoted as $E_0(R,\theta,\phi)$, which is 19.82 eV at the infinite distance between the $He^*(2\,^3S)$ atom and the molecule. By accumulating the electronic transition probability for the respective electron kinetic energy at each trajectory step, the collision-energy resolved PIES (CERPIES) was obtained.

Vibrational structures in CERPIES were constructed by distributing ionization probabilities according to the Franck–Condon factors and vibrational frequencies; for N_2 theoretical values[81] were used, and for CO[45] and CH_3CN[82] observed data for photoelectron spectra were employed. In this treat-

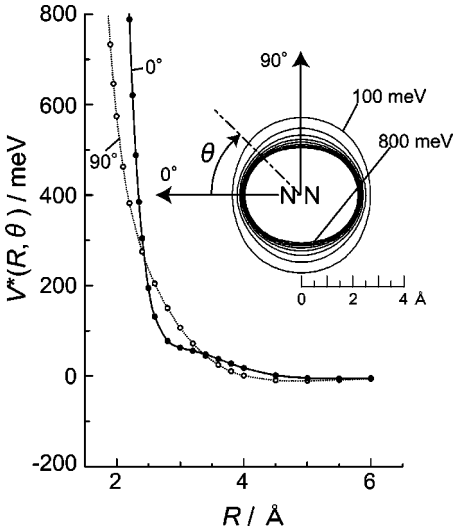

FIG. 1. The entrance potential energy curves $V^*(R,\theta)$ for $N_2+He^*(2\,^3S)$ obtained from the EC model potential calculations [see Eq. (6)]. Optimized parameter sets were listed in Table I. R is the distance between $He^*(2\,^3S)$ and the center-of-mass of N_2, and θ is the angle from the collinear direction. The contour maps for the repulsive boundary positions are shown with an energy spacing of 100 meV.

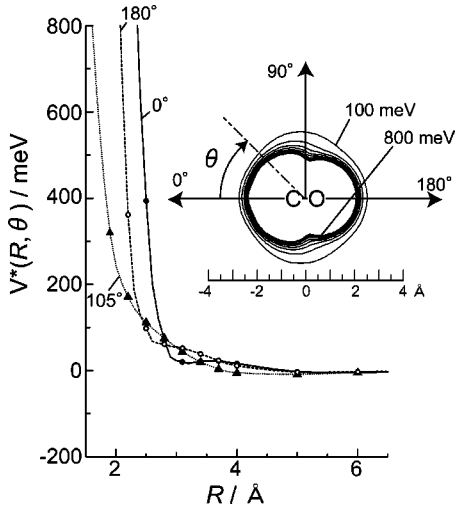

FIG. 2. The entrance potential energy curves $V^*(R,\theta)$ for CO $+He^*(2\,^3S)$ obtained from the EC model potential calculations [see Eq. (6)]. Optimized parameter sets were listed in Table I. R is the distance between $He^*(2\,^3S)$ and the center-of-mass (X) of CO, and θ denotes the CXHe* angle. The contour maps for the repulsive boundary positions are shown with an energy spacing of 100 meV.

ment, intramolecular potentials of the ion were assumed not modified by the presence of the He atom. The bandwidth of each vibrational peak was broadened by a Gaussian with a full-width at half-maximum (fwhm) of 155 meV, which was estimated from the apparatus function. Theoretical 2D-PIES was obtained from a number of CERPIESs with different collision energies in the interval of $E_c=10$ meV.

IV. RESULTS AND DISCUSSION

A. $N_2+He^*(2\,^3S)$ and $CO+He^*(2\,^3S)$

Figures 1 and 2 show the entrance potential energy curves $V^*(R,\theta)$ obtained from the EC model potential calculations. The contour maps for the repulsive boundary positions are also shown with an energy spacing of 100 meV. Parameters for the EC model were determined so as to reproduce observed CEDPICS as well as branching ratios.[59] Optimized parameter sets were listed in Table I. The nature of the obtained parameters will be discussed in Sec. IV D.

In the case of N_2+He^*, calculated model potential energies were positive almost all around the N_2 molecule, except for a very shallow van der Waals well. The calculated well depth is -9.22 meV at $R=4.88$ Å for the perpendicular direction ($\theta=90°$). For repulsive potentials, the intensity of 2D-PIES is expected to increase with increasing collision energy, because collision partners can interact more closely at higher collision energies to increase the ionization width. In the collision energy range larger than 80 meV, the repulsive potential wall for the collinear direction ($\theta=0°$) is much steeper than that for the perpendicular direction ($\theta=90°$). On the other hand, for collision energies below 80 meV the slope of the potential wall is considerably softened for $\theta=0°$. The origin of this ''soft spot'' has been discussed as the sp hybridization effect of atomic orbitals on He*(Li) atom.[19,38,83–86] It should be noted that the sp hybridization effect is also responsible for the very hard repulsive wall above 80 meV, since the downward deformation of the potential curve from a simple exponential decay at the distance of ca 2.5–3.5 Å explains both behaviors for $\theta=0°$.[19]

In the case of $CO+He^*$, calculated model potential energies were also almost all positive around the CO molecule. The calculated van der Waals well depth is -11.5 meV at $R=4.55$ Å for the almost perpendicular direction ($\theta=80.3°$). The repulsive potential wall for the collinear directions ($\theta=0°$ and $\theta=180°$) becomes steeper at the higher collision energy range than that for the perpendicular direction ($\theta=90°$). Although this propensity is similar to the case of N_2+He^*, crossover collision energies are 30 meV for $\theta=0°$(C-atom side) and 70 meV for $\theta=180°$(O-atom side) reflecting the anisotropy. This difference in the energy range of the soft spot, where the downward deformation effect occurs on the potential curve, is also related to the relative hardness of the potential wall at the higher energy region that causes the slope of the CEDPICS for the $\tilde{X}$ state being more flattened with respect to that for the $\tilde{B}$ state.

By collision with $He^*(2\,^3S)$, N_2 and CO molecules can be ionized into three ionic states. $\tilde{X}(^2\Sigma_g^+)$, $\tilde{A}(^2\Pi_u)$, and $\tilde{B}(^2\Sigma_u^+)$ states of N_2^+ correspond to the removal of an electron from the $3\sigma_g$, $1\pi_u$, and $2\sigma_u$ molecular orbitals of N_2,

TABLE I. Optimized parameters A_i and B in the correction term of $A_iP_i(\cos\theta)\exp(-R/B)$ [see Eq. (6)] for $N_2+He^*(2\,^3S)$ and CO $+He^*(2\,^3S)$.

	$N_2+He^*(2\,^3S)$	$CO+He^*(2\,^3S)$
A_0/meV	941 (±5)[a]	2870 (±3)[a]
A_1/meV	⋯	296 (±4)[a]
A_2/meV	-379 (±7)[a]	-1300 (±4)[a]
A_4/meV	0 (±7)[a]	⋯
B/Å	1.104 (±0.014)[a]	0.861 (±0.009)[a]

[a]Estimated uncertainties in Ref. 59.

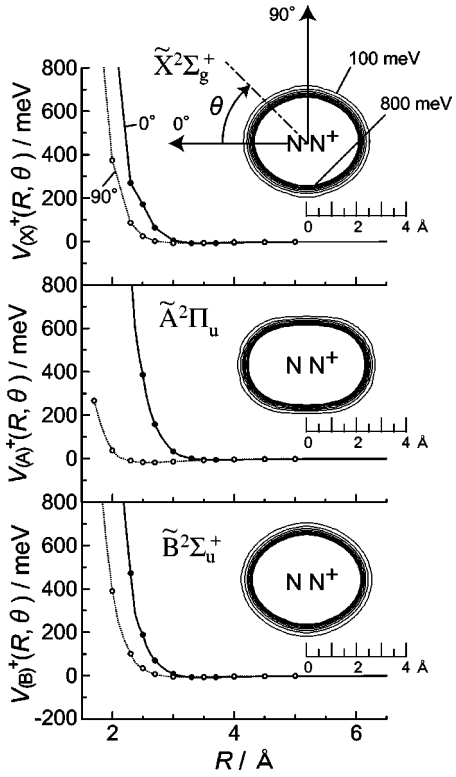

FIG. 3. The calculated exit potential energy curves $V^+_{(i)}(R,\theta)$ for $N_2^+ + He$. R is the distance between He and the center-of-mass of N_2^+, and θ is the angle from the collinear direction. The contour maps for the repulsive boundary positions are also shown with an energy spacing of 100 meV. $\tilde{X}(^2\Sigma_g^+)$, $\tilde{A}(^2\Pi_u)$, and $\tilde{B}(^2\Sigma_u^+)$ denote the electronic states of N_2^+.

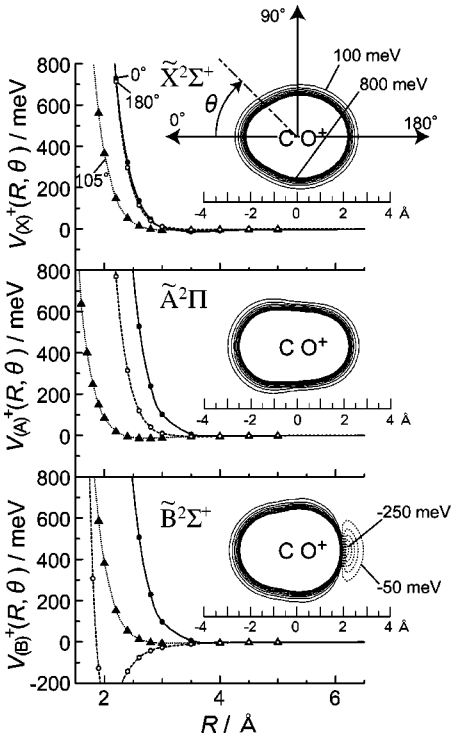

FIG. 4. The calculated exit potential energy curves $V^+_{(i)}(R,\theta)$ between CO^+ and He. R is the distance between He and the center-of-mass (X) of CO^+, and θ denotes the CXHe angle. The contour maps for the repulsive boundary positions are also shown with an energy spacing of 100 meV. $\tilde{X}(^2\Sigma^+)$, $\tilde{A}(^2\Pi)$, and $\tilde{B}(^2\Sigma^+)$ denote the electronic states of CO^+.

respectively. For CO^+, $\tilde{X}(^2\Sigma^+)$, $\tilde{A}(^2\Pi)$, and $\tilde{B}(^2\Sigma^+)$ states correspond to ionization from the 5σ, 1π, and 4σ molecular orbitals of CO, respectively. Figures 3 and 4 show the exit potential energy curves $V^+_{(i)}(R,\theta)$ for $N_2^+ + He$ and $CO^+ + He$. The contour maps for the repulsive boundary positions are also shown with an energy spacing of 100 meV. Exit potentials are repulsive except for $CO+(\tilde{B}\,^2\Sigma^+)$. As can be seen from a comparison of the contour maps, the repulsive wall in each exit potential is much harder than that of the entrance potential; geometrical spacing of the contour curves are very narrow in every direction for V^+. This is probably due to the very small polarizability of the ground state He atom. It should be noted that positions of the repulsive walls for the exit potential are compressed to the shorter distances in the directions where ionized electron orbitals are distributed; positions of the repulsive walls for the $\tilde{A}$ states are extremely compressed at the shorter distances in the perpendicular directions both in $N_2^+ + He$ and $CO^+ + He$.

Figures 5 and 6 show (a) observed and (b) calculated contour maps of 2D-PIES; heights of electron signals or cross sections are shown in a relative unit. The right-hand panel of each figure shows CERPIES drawn with a solid line for $E_c \sim 100$ meV and with a dotted line for $E_c \sim 300$ meV for $N_2 + He^*(2\,^3S)$ or $E_c \sim 250$ meV for $CO + He^*(2\,^3S)$. In order to reproduce observed branching ratios, the ratios of the constant $K^{(i)}$ in Eq. (11) were optimized as $K^{(\tilde{X})}:K^{(\tilde{A})}:K^{(\tilde{B})} = 1.00:1.33:2.38$ for $N_2 + He^*$ and $K^{(\tilde{X})}:K^{(\tilde{A})}:K^{(\tilde{B})} = 1.00:2.07:2.55$ for $CO + He^*$. Collision energy dependences of band intensities, peak positions, and bandwidths are well reproduced by the present trajectory calculations.

The collision energy dependence of the band intensity in 2D-PIES shows strong anisotropy of the entrance potential surface, because the electronic transition in Penning ionization effectively occurs when a He* atom approaches to a geometrical region where the electron density of the molecular orbital to be ionized is relatively high [see Eq. (11)]. Figures 7 and 8 show $\log \sigma^{(i)}$ versus $\log E_c$ plots of CEDPICS for $N_2 + He^*(2\,^3S)$ and $CO + He^*(2\,^3S)$. Observed cross sections are plotted with circles and total cross sections are normalized with crossed-beam experiments,[17] and they are compared with those for the present calculation shown with solid lines. Contour maps of the electron densities for molecular orbitals corresponding to the respective ionic states are also shown in Figs. 7 and 8, in which the thick solid line in the maps shows the contour curve of 100 meV of the entrance potential as a reference of the repulsive boundary. In the maps of the molecular orbitals and the repulsive boundary, the thick arrow indicates important directions of the interactions between the molecule and the He* atom. The most reactive directions are in the perpendicular directions for Π states and the collinear directions for Σ states reflecting respective orbital electron distributions. It is of note that for the Π state $(\tilde{A})$ of $N_2 + He^*(2\,^3S)$ the most reactive directions change from ca. 50° to 90° on going from 100 to 400 meV. This unusual behavior is related to the dramatic change of the outer shape of the boundary surface for

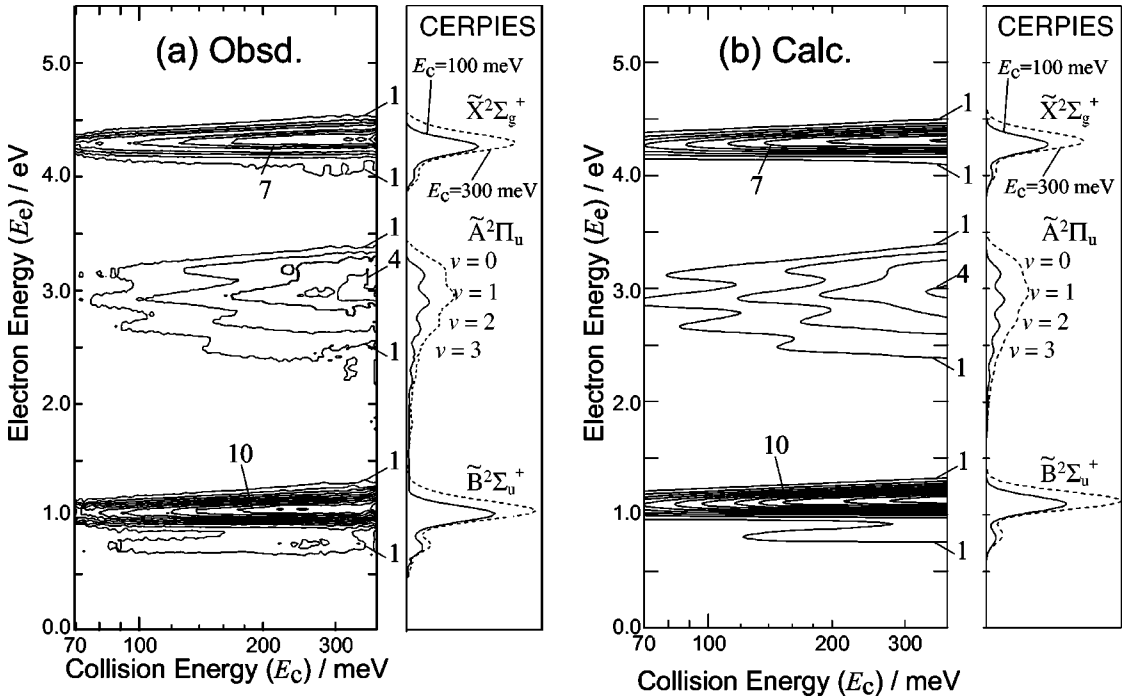

FIG. 5. (a) Observed and (b) calculated two-dimensional Penning ionization electron spectra (2D-PIES) for $N_2+He^*(2\,^3S)$ in a relative unit. The right-hand panel of each figure shows CERPIES drawn with a solid line for $E_c=100$ meV and with a dotted line for $E_c=300$ meV.

N_2 with $He^*(2\,^3S)$ from the oblate form to the prolate form with increasing energies, as can be seen in Fig. 1. Intensities of $\tilde{A}$ states for both N_2+He^* and $CO+He^*$ increase more rapidly with the increase of E_c than $\tilde{X}$ or $\tilde{B}$ state, which reflects the softness of the repulsive potentials towards perpendicular directions of molecular axis in the collision energy range of the present study. CEDPICS for $\tilde{X}$ and $\tilde{B}$ states (Σ states) are nearly the same for N_2+He^*,[19,42,44,59] reflecting the electron distribution of respective σ orbitals ($3\sigma_g$ and $2\sigma_u$) being very similar to the collinear directions ($\theta=0°$). In the case of $CO+He^*$, CEDPICS for $\tilde{X}$ and $\tilde{B}$ states (Σ states) are on the other hand considerably different,[45,59] because of the difference of the electron distribution of the corresponding σ orbitals (5σ and 4σ); the exterior electron

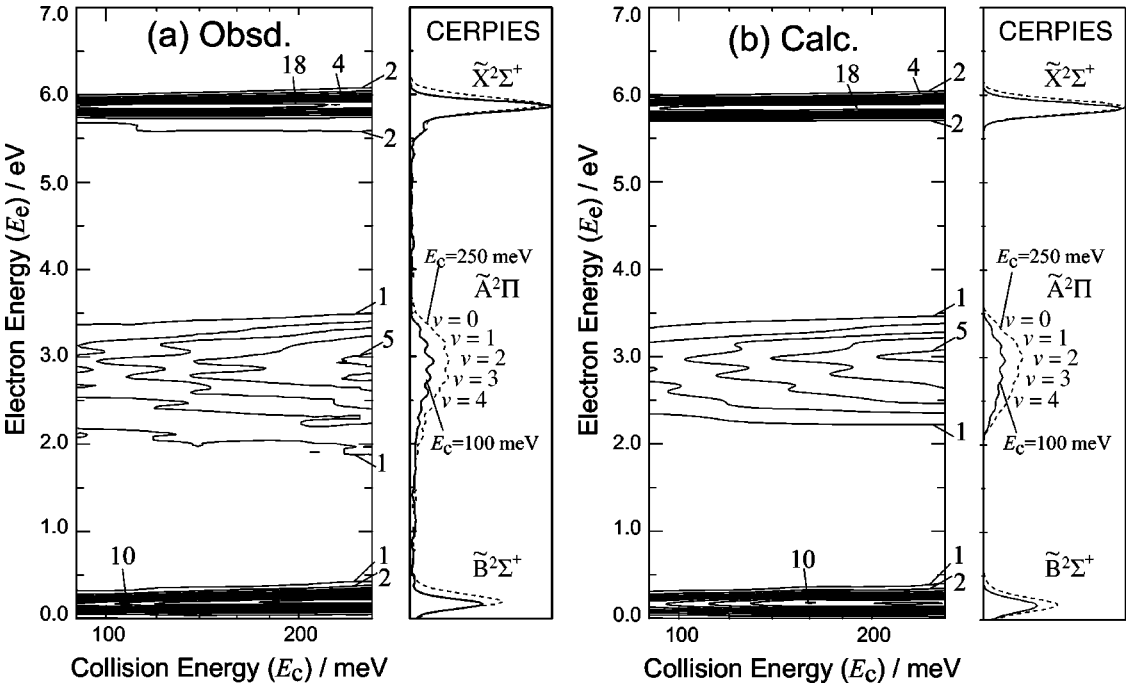

FIG. 6. (a) Observed and (b) calculated 2D-PIES for $CO+He^*(2\,^3S)$ in a relative unit. The right-hand panel of each figure shows CERPIES drawn with a solid line for $E_c=100$ meV and with a dotted line for $E_c=250$ meV.

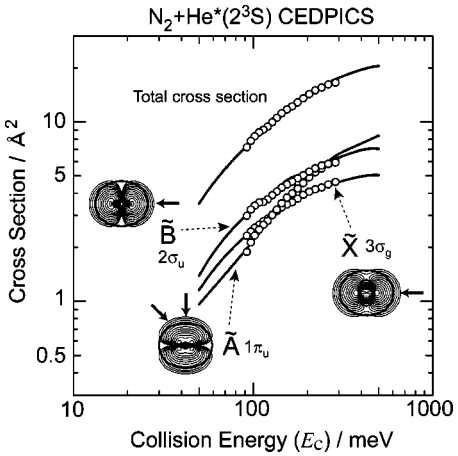

FIG. 7. The $\log \sigma^{(i)}$ vs $\log E_c$ plots for $N_2+He^*(2\,^3S)$. Observed cross sections are plotted with circles, the present calculation drawn with solid lines. Contour maps of the electron densities for molecular orbitals corresponding to the respective ionic states are also shown. Observed total cross sections are normalized to the reported value (Ref. 17) at $E_c=200$ meV.

distribution is dominant at the C-atom side for 5σ orbital and at the O-atom side for 4σ orbital. Since the repulsive wall for $\theta=0°$ is much more hardened than that for $\theta=90°$ in the energy range between 180 and 40 meV in connection with the lower soft spot for $\theta=0°$, the slope of the CEDPICS for $\tilde{X}$ state of CO^+ is more flattened. These characteristics can be seen in the both observed and calculated CERPIES in Fig. 6.

Peak positions of the most prominent peaks in observed and calculated PIES are listed in Table II at the lower and higher collision energies, $E_c=100$ and 300 meV for N_2+He^* and $E_c=100$ and 250 meV for $CO+He^*$. Full-widths at half-maxima are also listed for $\tilde{X}$ and $\tilde{B}$ states in parentheses. The calculated peak positions are in good agreement with the observed values within 10–60 meV. It was found that the calculated peak positions are insensitive to the exit potentials; even if the exit potentials are artificially replaced

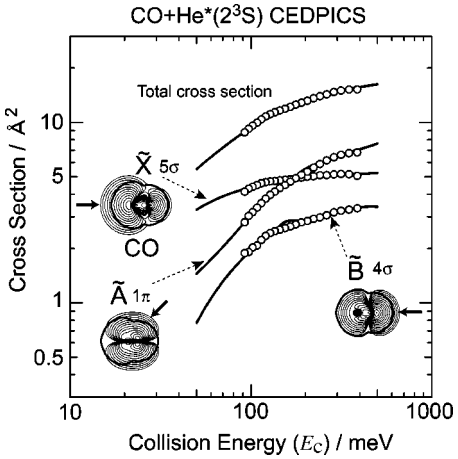

FIG. 8. The $\log \sigma^{(i)}$ vs $\log E_c$ plots for $CO+He^*(2\,^3S)$. Observed cross sections are plotted with circles, the present calculation drawn with solid lines. Contour maps of the electron densities for molecular orbitals corresponding to the respective ionic states are also shown. Observed total cross sections are normalized to the reported value (Ref. 17) at $E_c=100$ meV.

TABLE II. Peak positions (eV) of the most prominent vibrational band in CERPIES ($E_c=100$, 300 meV for N_2+He^* and $E_c=100$, 250 meV for $CO+He^*$). Full-widths at half-maxima (meV) are also shown for $\tilde{X}$ and $\tilde{B}$ states in parentheses. Peak positions of $\tilde{A}$ states are those of $\nu=1$ for N_2+He^* and $\nu=2$ for $CO+He^*$.

		E_c	$\tilde{X}$	$\tilde{A}$	$\tilde{B}$
N_2+He^*	Obsd.	100	4.26 (163)	2.90	1.04 (165)
		300	4.30 (200)	2.96	1.07 (203)
	Calc.	100	4.28 (167)	2.90	1.10 (165)
		300	4.31 (196)	2.97	1.12 (189)
$CO+He^*$	Obsd.	100	5.86 (151)	2.95	0.17 (142)
		250	5.89 (192)	2.97	0.20 (181)
	Calc.	100	5.85 (164)	2.97	0.17 (183)
		250	5.86 (196)	3.00	0.17 (201)

by a completely flat potential, the calculated peak positions coincide within 10 meV. This indicates that the vertical ionization transition from the entrance potential occurs mostly onto the flat area of the exit potential. This is highly likely, since the repulsive walls for the exit channel are very much compressed to the shorter distance in comparison with the entrance channel as mentioned above for Figs. 3 and 4. It should be noted that the calculated peak positions are slightly overestimated by 10–60 meV. This indicates that entrance potentials especially at the lower repulsive parts may still be overestimated by this amount. The observed peak energy shift ΔE estimated with respect to the energy difference between the metastable excitation energy (19.82 eV) and the target IP is at most 60 meV with $E_c=100$ meV, which indicates that the ionization probabilities do not governed by the trajectories with zero-impact parameters. As for the bandwidths, calculations explain the observation qualitatively; the bandwidths increase with increasing collision energies. Since the increases of the bandwidths are 20–40 meV and much smaller than the increments of the collision energy of 200 meV (N_2) or 150 meV (CO), the ionization transitions do not mainly occur on the highest turning points corresponding to the zero-impact parameter. This is consistent with the previous analyses of ionization probabilities as functions of impact parameter values.[42]

B. $CH_3CN+He^*(2\,^3S)$

Figure 9 shows the contour map of the calculated model potential energy surface V_0 for CH_3CN+He^*, taken in the σ_v plane ($\phi=0°$), which includes one of CH bonds in the

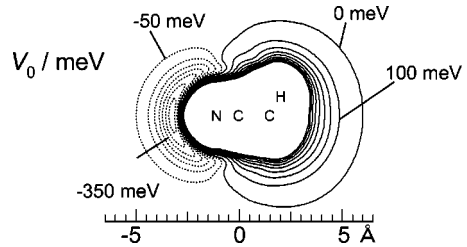

FIG. 9. The contour map of the calculated model potential energy surface V_0 for $CH_3CN+He^*(2\,^3S)$ taken in the σ_v plane ($\phi=0°$). The spacing of the contour lines is 50 meV for negative values and 100 meV for positive values between 0 and 800 meV, respectively.

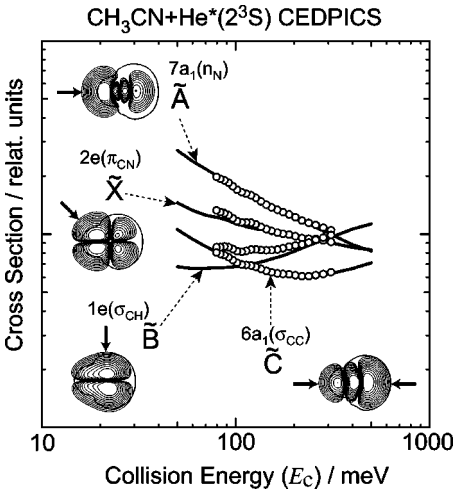

FIG. 10. The $\log \sigma^{(i)}$ vs $\log E_c$ plots for $CH_3CN+He^*(2\,^3S)$. Observed cross sections are plotted with circles in a relative unit, the present calculation drawn with solid lines. Contour maps of the calculated ionization widths corresponding to the respective ionic states are also shown.

methyl group. The spacing of the contour lines is 50 meV for negative values and 100 meV for positive values between 0 and 800 meV, respectively. A CH_3CN molecule interacts attractively with $He^*(2\,^3S)$ when a He* atom approaches the N atom. The well depth is about 380 meV located on the coaxial line of the CN bond. The presence of a deep potential well around the CN group was also found for an end-on-type complex of CH_3CN+Li in the earlier studies.[54,55]

Figure 10 shows $\log \sigma^{(i)}$ versus $\log E_c$ plots of CEDPICS for $CH_3CN+He^*(2\,^3S)$. Observed cross sections are plotted with circles in a relative unit, and they are compared with those for the present calculation shown with solid lines. The ionic states of CH_3CN^+, $\tilde{X}(1\,^2E)$, $\tilde{A}(1\,^2A_1)$, $\tilde{B}(2\,^2E)$, and $\tilde{C}(2\,^2A_1)$ states, correspond to the ionization from the $2e(\pi_{CN})$, $7a_1(n_N)$, $1e(\sigma_{CH})$, and $6a_1(\sigma_{CC})$ molecular orbitals of CH_3CN, respectively. Contour maps of the calculated ionization widths corresponding to the respective ionic states are also shown in Fig. 10, in which the thick solid line in the maps shows the contour curve of 100 meV of the entrance potential as a reference of the repulsive boundary. In the maps of the ionization widths and the repulsive boundary, the thick arrow indicates important directions of the interactions between CH_3CN molecule and the He* atom.

In order to reproduce branching ratios, the ratios of the constant $K^{(i)}$ of Eq. (11) were optimized as $K^{(\tilde{X})}:K^{(\tilde{A})}:K^{(\tilde{B})}:K^{(\tilde{C})}=1.00:1.83:5.16:9.89$. After this optimization, calculated CEDPICS as well as branching ratios were found to be in good agreement with the experiment, although the lower energy part of the $\tilde{B}$ state is less satisfactory, which will be discussed below in connection with the quality of the entrance model potential. The slopes m in $\log \sigma^{(i)}$ versus $\log E_c$ plots are listed in Table III. Negative values of the slopes m can be ascribed to attractive interactions around the potential well in the entrance surface.[43] The largest negative slope for the $\tilde{A}$ state is clearly related to the deep potential well around the N-atom end of the CN group where the electron distribution of the corresponding molecular orbital $[7a_1(n_N)]$ is most distributed. The second largest negative slope m for the $\tilde{X}$ state is also reasonable, since the electron distribution of the corresponding molecular orbital (π_{CN}) is also dominant around the attractive potential well region. The slope value m for the $\tilde{B}$ state is positive for both observed and calculated CEDPICS, though the latter is much larger. Since the exterior electron distribution of the $1e(\sigma_{CH})$ orbital is extending around the border between the attractive well on the CN group and the repulsive walls around the CH_3 group. Considering that the Li model potential is likely to overestimate repulsive energies as found in the previous studies,[19,42,43] the discrepancy may be improved when the Li model potential is modified. As for the $\tilde{C}$ state corresponding to $6a_1(\sigma_{CC})$ orbital, the calculation has yielded an excellent agreement with the newly obtained experimental data in the present study. The most important geometries for the $\tilde{C}$ state are in axial directions as indicated in Fig. 10. A long these directions, entrance potentials are highly attractive or repulsive and not in the marginal regions like the case of the B state, to which calculations depend crucially on the qualities under subtle balances.

TABLE III. Slopes m in $\log \sigma^{(i)}$ vs $\log E_c$ plot of $CH_3CN+He^*(2\,^3S)$ in the collision energy range from 90 to 300 meV.

Ionic state	Experiment	Calculation
$\tilde{X}(1\,^2E)$	−0.26	−0.20
$\tilde{A}(1\,^2A_1)$	−0.47	−0.50
$\tilde{B}(2\,^2E)$	0.12	0.31
$\tilde{C}(2\,^2A_1)$	−0.30 (90–170 meV)	−0.32 (90–170 meV)
	−0.01 (170–300 meV)	0.00 (170–300 meV)

Exit potentials are much harder than the entrance potential, as shown in Fig. 11. This is probably due to the small polarizability and the compact wave function of the He atom. The repulsive walls are more compressed to the shorter distances at the directions where ionized electron orbitals are mainly distributed. Since repulsive boundaries for the ionized surfaces are much more compressed in comparison with the entrance surface, the exit potentials are almost flat in the region where the He* atom effectively interact with the collision partner on the entrance repulsive surface. This propensity is, however, relative. Around the CN group, there is a deep well in the entrance surface. In this region, the respective exit surface cannot be considered as a flat surface. This point will be discussed in connection with the effects of the exit potential on the calculated 2D-PIES.

Figure 12 shows (a) observed and (b) calculated contour maps of 2D-PIES. The right-hand panel of each figure shows CERPIES drawn with a solid line for $E_c \sim 100$ meV and a dotted line for $E_c \sim 250$ meV. Table IV lists the peak position of $\tilde{X}(1\,^2E)$ and $\tilde{A}(1\,^2A_1)$ states and peak energy shifts ΔE in parentheses; ΔE were estimated with respect to the energy difference between the metastable excitation energy (19.82 eV) and the target IP.

As can be seen from Fig. 12 and Table IV, the following experimental features are qualitatively well reproduced by the present trajectory calculations:

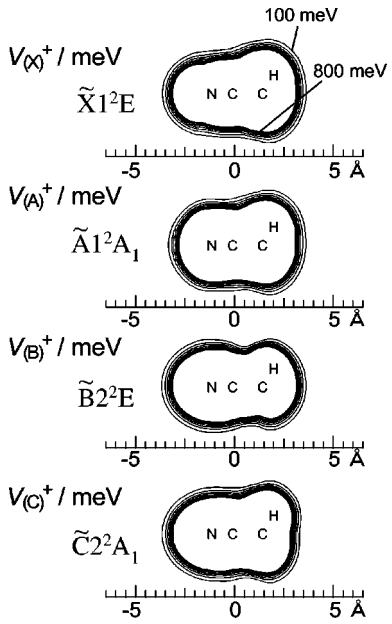

FIG. 11. The calculated exit potential energy curves $V_{(i)}^+$ for $CH_3CN^+ + He$ taken in the σ_v plane ($\phi=0°$). The contour maps for the repulsive boundary positions are also shown with an energy spacing of 100 meV. $\tilde{X}(1\,^2E)$, $\tilde{A}(1\,^2A_1)$, $\tilde{B}(2\,^2E)$, and $\tilde{C}(2\,^2A_1)$ denote the electronic states of CH_3CN^+.

(i) The peak energy shifts ΔE are negative for $\tilde{X}(1\,^2E)$ and $\tilde{A}(1\,^2A_1)$ states.
(ii) The negative peak energy shift ΔE of $\tilde{X}(1\,^2E)$ is larger than that of $\tilde{A}(1\,^2A_1)$.
(iii) Bandwidths of $\tilde{X}(1\,^2E)$ and $\tilde{B}(2\,^2E)$ states are increasing and slightly expanded to the higher E_e side with the increase of E_c.

TABLE IV. Peak position of $\tilde{X}(1\,^2E)$ and $\tilde{A}(1\,^2A_1)$ states of CH_3CN^+. The peak energy shift estimated with respect to the energy difference between the metastable excitation energy (19.82 eV) and the target ionization potential is also shown in parentheses in a meV unit.

	Ionization potential[a]/eV	E_c	Obs.	Calc.
$\tilde{X}(1\,^2E)$	12.20	100	7.16 (−460)	7.30 (−320)
		250	7.16 (−460)	7.30 (−320)
$\tilde{A}(1\,^2A_1)$	13.13	100	6.36 (−330)	6.43 (−260)
		250	6.36 (−330)	6.43 (−260)

[a]Reference 82.

(iv) The peak positions of the $\tilde{A}(1\,^2A_1)$ and $\tilde{X}(1\,^2E)$ states are independent of E_c.
(v) The intensities and widths increase on going to the higher E_c side for the band of $\tilde{B}(2\,^2E)$ state.
(vi) The intensities and widths show minima at an intermediate collision energy for the band of $\tilde{C}(2\,^2A_1)$ state.

From the more quantitative analyses, the following features should be noted:

(1) The calculated negative peak energy shift ΔE of $\tilde{X}(1\,^2E)$ state is smaller than the observed value by 140 meV.
(2) The calculated low E_e components for the band of $\tilde{X}(1\,^2E)$ are too small.
(3) The calculated positive slope in log $\sigma^{(i)}$ versus log E_c plot of $\tilde{B}(2\,^2E)$ is too large, as mentioned for the CEDPICS in Fig. 10.

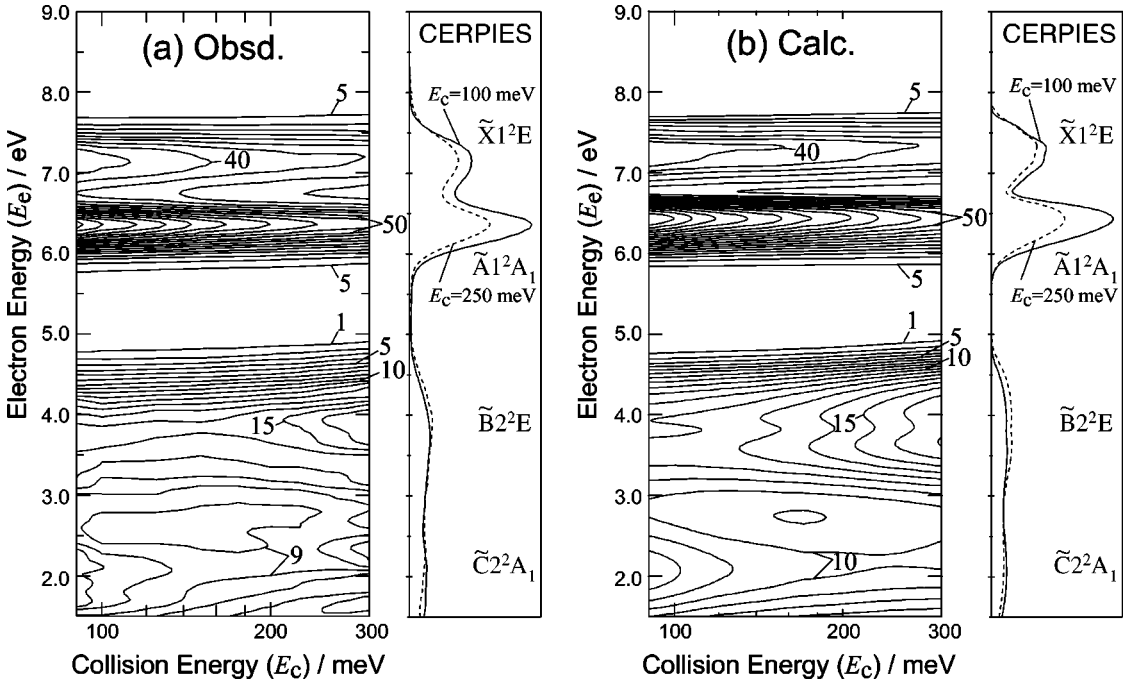

FIG. 12. (a) Observed and (b) calculated 2D-PIES for $CH_3CN + He^*(2\,^3S)$ in a relative unit. The right-hand panel of each figure shows CERPIES drawn with a solid line for $E_c = 100$ meV and with a dotted line for $E_c = 250$ meV.

These features are related to the deficiency of the Li model potential of the entrance potentials, especially in the directions where repulsive and attractive interactions compete with each other; such regions are located around the perpendicular direction of the CCN axis or CH bond where $2e(\pi_{CN})$ and $1e(\sigma_{CH})$ orbitals are expanding outside. This will be discussed in connection with the quality of the entrance model potentials in Sec. IV D.

C. Influence of the exit potential on 2D-PIES

Crucial influences of exit potentials on 2D-PIES were not found except for the $\tilde{X}(1\,^2E)$ and $\tilde{A}(1\,^2A_1)$ states of CH_3CN^+. This is easily understood by the ionic surfaces being much more compressed than the entrance surfaces. The exceptions of the $\tilde{X}(1\,^2E)$ and $\tilde{A}(1\,^2A_1)$ states are related to the very deep well around the CN group in the entrance surface. Since the repulsive boundary in this region for the entrance surface can be compressed too much, even more than the ionic state potentials, the situation may be reversed. In order to confirm this effect of an overcompression of the repulsive potential in the entrance surface, artificial calculations were performed using completely flat exit potentials. The results of the 2D-PIES with flat exit potentials were found to be very similar to the normal results in Fig. 12 except for the $\tilde{X}(1\,^2E)$ and $\tilde{A}(1\,^2A_1)$ states; The peak position for the $\tilde{X}(1\,^2E)$ state was shifted to the higher electron energy by ca. 50 meV and lower electron energy tails for the $\tilde{A}(1\,^2A_1)$ state were cut off to a very wide range of ca. 400 meV. This clearly indicates the importance of the qualities of exit potentials where the entrance potential has a deep well. In view of this, if the repulsive boundaries around the CN group in the exit potentials for the $\tilde{X}(1\,^2E)$ and $\tilde{A}(1\,^2A_1)$ states are much more compressed, the peak positions for these bands as well as the lower E_e tail for the band of the $\tilde{A}(1\,^2A_1)$ state will be improved.

D. Remarks on the entrance model potentials

In connection with the entrance potentials, there are several important points to be mentioned. In the *ab initio* determination of interaction potentials, basis functions should be carefully chosen. At a minimum level, split-valence basis sets with diffuse and polarization functions should be used.[87] Full counterpoise corrections need to be made to account for basis-set superposition errors.[65] Effects of electron correlation are also important. A comparison has been made for MP2, CCSD(T), and QCISD(T) levels.[88] The CCSD(T) level is recommended for small systems, and at least MP2 corrections should be made for the larger systems. The present study followed this criterion. In addition to the problems associated with basis functions and electron correlation, the use of the Li model causes some inaccuracies. In order to compensate for these drawbacks, a linear scaling treatment of $V_0^{\text{scaled}}=aV_0$ has been employed in the previous studies for N_2+He^*[42,44] and $CO+He^*$.[45] It should be noted that the optimized values for the parameter a are smaller than unity, indicating overestimation of repulsive interactions or underestimation of attracting interactions; $a=0.50$ for N_2 with an MP2/6-311+G* level,[42] $a=0.80$ for N_2 with a CCSD(T)/6-311+G* level,[44] and $a=0.55$ for CO with a CCSD(T)/6−311+G* level.[45] It is also of note that the CCSD(T) treatment improves electron correlation effects to give a larger value for the parameter a much closer to unity than the MP2 calculation.

In the present study a more flexible form of Li model potentials than the simple linear scaling has been used for N_2 and CO. The aim of this treatment is to obtain much better quantitative agreement with the observation, especially for CO. In the case of CO, the C-atom side and O-atom side should have different characteristics. Thus, the simple scaling treatment should be replaced by the more flexible functions V_{EC} using exponential corrections combined with Legendre expansions in Eq. (6).[59] Improved aspects in comparison with the simple scaling results are summarized as follows in connection with the optimized parameter sets in Table I:

(1) The slopes for the $\log\sigma^{(i)}$ versus $\log E_c$ plots of CEDPICS for CO are considerably flattened in the lower collision energy range below 150 meV to give excellent agreement with the experiments. This effect is especially remarkable in the calculated CEDPICS for the X state of CO^+. This has a connection with the optimized positive value of $A_1=296$ meV for CO in Table I, which draws down the repulsive parts of potentials more effectively on the C-atom side around $\theta=0°$.
(2) The slopes for the $\log\sigma^{(i)}$ versus $\log E_c$ plots of CEDPICS for N_2 are also improved in the lower collision energy range, although the effects are not remarkable as in the case of CO. This is also related to the downward deformation effects of the entrance potential in the lower parts.

Concerning the optimized values of (A_0,A_2,A_4) in Table I, the spherical term A_0 is the largest for both N_2 and CO. Isotropic contributions of inaccuracies due to basis functions or electron correlation effects can be corrected with this term to some extent. It should be noted that A_2/A_0 has a negative value of ca. -0.4, which indicates oblate corrections leading to the more negative contributions drawing down the interaction potentials effectively in the perpendicular directions where π electrons distribute. This indicates that a charge transfer (CT) interaction leading to M^-A^{*+} is responsible for the dominant contributions in the corrections to the Li model potentials V_0; the $2s$ electron in a He*(Li) atom tends to be transferred into the degenerate antibonding π orbitals in N_2 and CO. Although the CT interaction of M^-A^{*+} is already included in the V_0, the optimized A_2/A_0 values clearly show the *ab initio* Li model potential is deficient to a certain extent in inclusion of the CT interaction. It is well known that the magnitude of interactions is enhanced when the energy separation between interacting orbitals becomes smaller. Since the ionization energy of $Li(2\,^2S)(5.392\,eV)$ is larger than that of $He^*(2\,^3S)\times(4.768\,eV)$, the Li model potential underestimates the CT interaction. Therefore, the positive value of A_1 in Table I indicates that corrections are larger on the C-atom side, because of the distribution of the antibonding π orbitals being

much more localized on the C-atom side. Relevance of the CT interaction with target unoccupied orbitals can also be rationalized by the following arguments on the B parameter. The optimized values for the B parameter in Table I are 1.104 Å for N_2 and 0.861 Å for CO, respectively. The characteristic length B can be connected with the asymptotic behavior of wave function tails known as $B^{-1}=2(2I)^{1/2}$, where I is the ionization potential.[89] The characteristic length of ca. 1 Å corresponds to an orbital function whose ionization potential is ca. 1 eV, which is of approximate order of unoccupied molecular orbitals. It is of note that the present B values of ca. 1 Å are in good agreement with the corresponding values of $B=0.909$ Å ($B^{-1}=1.10$ Å^{-1}) in the exponential CT interaction term for the system of CH_3Cl+Ne^* by Albertí *et al.*,[90] which has been introduced in addition to the van der Waals terms in traditional semiempirical potentials.

In connection with the qualities of Li model potentials, a precise estimate has been made for atomic targets by Hotop *et al.*;[53] the well depths for Li+X (X=H, Li, Na, K, Hg) systems were found to be 10% to 20% larger than those for $He^*(2\,^3S)+X$. Although this estimate of inaccuracies involved in the Li model seems to be opposite to those deduced in the present and previous studies for molecular targets,[42–45,59] the key points are the major interactions involved in the atomic targets; the most important role is possessed by the unpaired valence electron of the atom, whose energy level is not higher than the $2s$ electron of the Li atom to lead to overestimation of the interactions in comparison with the more higher $2s$ electron of He*. This argument also supports the propensity that Li model potentials have been rather satisfactory for larger systems having a deep potential well, since in these systems occupied molecular orbitals play important roles in interaction with the Li(He*) atom to lead to larger attractive interactions for the Li model, compensating the drawbacks to some extent. However, even for systems such as CH_3CN, the effects of CT interactions involving unoccupied target orbitals are important, since the lower energy parts of repulsive walls in the entrance potentials may be improved to give the better CEDPICS and CERPIES for ionic states whose respective orbitals having electron densities in the relevant spatial regions as in the case of $\tilde{X}(1\,^2E)$ and $\tilde{B}(2\,^2E)$ states in the present study.

E. Remarks on the ionization width

Although the present estimation of the ionization width $\Gamma^{(i)}$ by Eq. (11) was found to be excellent for taking the anisotropy and the radial dependence into account quantitatively, optimized values for constants $K^{(i)}$ in Eq. (11) should be discussed. In Table V, optimized values for $K^{(i)}$ are listed and compared with the ionization potential of the respective ionic state. There is a tendency that the larger the IP of the ionized electron (the smaller the kinetic energy of ejected electron E_e), the larger the corresponding values for $K^{(i)}$ become. This is at least partly related to a factor of $2\pi\rho^{(i)}$ in Eq. (7) for the fundamental equation for the ionization width. When expanding outgoing electron wave functions into partial waves, this factor is normalized as $2\pi\rho^{(i)}=4(2E_e)^{-1/2}$.[29] Moreover, two electron integrals related to electron transfer or electron exchange may have larger values when the energy gap becomes smaller; the energy gap to be considered is the difference between the IP of the He $1s$ orbital and the IP of the respective target molecular orbital. Since this effect is missing in Eq. (11) after employing the Mulliken approximation and using overlap integrals, the values of $K^{(i)}$ should also become larger for the larger IP states. Based on these arguments, the tendency in Table V that the smaller E_e (the larger IP) the larger $K^{(i)}$ can be considered to be reasonable.

TABLE V. The optimized relative ratios of $K^{(i)}$ of Eq. (11) and its corresponding molecular orbital energy.

Molecule	Ionic state	Relative ratio of $K^{(i)}$	Ionization potential[a] (eV)
N_2	$\tilde{X}(^2\Sigma_g^+)$	1.00	15.60
	$\tilde{A}(^2\Pi_u)$	1.33	16.75
	$\tilde{B}(^2\Sigma_u^+)$	2.38	18.78
CO	$\tilde{X}(^2\Sigma^+)$	1.00	14.01
	$\tilde{A}(^2\Pi)$	2.07	16.54
	$\tilde{B}(^2\Sigma^+)$	2.55	19.72
CH_3CN	$\tilde{X}(1\,^2E)$	1.00	12.20
	$\tilde{A}(1\,^2A_1)$	1.83	13.13
	$\tilde{B}(2\,^2E)$	5.16	15.13
	$\tilde{C}(2\,^2A_1)$	9.89	17.58[b]

[a]Adiabatic ionization potentials taken from Refs. 63 and 82.
[b]Vertical ionization potential.

V. CONCLUSION

In order to elucidate collisional reaction dynamics, collision energy dependence of partial ionization cross sections (CEDPICS) and collision-energy resolved Penning ionization spectra (CERPIES) were studied by 2D-PIES experiments and classical trajectory calculations based on *ab initio* molecular orbital calculations. The entrance potential embedded in the ionization continua can be approximated by replacing an excited $He^*(2\,^3S)$ atom by a ground state $Li(2\,^2S)$ atom. This treatment is satisfactory to estimate anisotropy and radial dependence of the entrance potential surface in good quantitative accuracy. Optimization of the Li model potential with additional correction functions revealed that CT interactions of the valence $2s$ electron in the He* atom with unoccupied molecular orbitals in the target molecule tend to be underestimated in the Li model, since the energy level of the $2s$ electron is lowered in the $Li(2\,^2S)$ atom by ca. 0.6 eV, in comparison with the $He^*(2\,^3S)$ atom. Corrections of this effect were found to be important for $N_2+He^*(2\,^3S)$ and $CO+He^*(2\,^3S)$, because the lower energy parts of repulsive walls in the entrance surfaces play decisive roles in the collision dynamics.

The exit potential surfaces were found to be much less important in collisional ionization dynamics. CEDPICS are irrelevant to the exit potentials. Even for CERPIES exit potentials are not important, because ion–molecule interactions are much stronger than the atom–molecule interactions to make the former potentials much more compact than the latter. This means that vertical transitions from the entrance

surface occur on almost flat parts of ionic surfaces. Some exceptional cases were found for $CH_3CN+He^*(2\,^3S)$; in this case there is a deep well of ca. 380 meV around the CN group that compresses the entrance repulsive surface to a large extent; thus, ionization transitions from the entrance surface at geometrical positions around the CN group occur on the nonflat parts of the exit surfaces.

Anisotropy and radial dependence of ionization widths $\Gamma^{(i)}$ were found to be essentially important to describe collision dynamics related to CEDPICS and CERPIES. The approximation of $\Gamma^{(i)}$ using overlap integrals between ionized target molecular orbital and He 1*s* orbital was found to be satisfactory. The proportionality constant $K^{(i)}$ in the expression of $\Gamma^{(i)}$ was found to have a correlation with the energy of the ejected electron.

ACKNOWLEDGMENTS

The present work was supported partly by a Grant-in-Aid for Scientific Research from the Japanese Ministry of Education, Science, and Culture. The authors appreciate the efforts by Dr. T. Ogawa in producing a program for trajectory calculations. They also thank Professor K. Takeshita for comparative studies of ionic state potentials.

[1] F. M. Penning, Naturwissenschaften **15**, 818 (1927).
[2] V. Čermák, J. Chem. Phys. **44**, 3781 (1966).
[3] A. Niehaus, Adv. Chem. Phys. **45**, 399 (1981).
[4] A. J. Yencha, in *Electron Spectroscopy: Theory, Techniques and Applications*, edited by C. R. Brundle and A. D. Baker (Academic, New York, 1984), Vol. 5.
[5] H. Hotop and A. Niehaus, Z. Phys. **228**, 68 (1969).
[6] K. Ohno, H. Mutoh, and Y. Harada, J. Am. Chem. Soc. **105**, 4555 (1983).
[7] K. Ohno, S. Matsumoto, and Y. Harada, J. Chem. Phys. **81**, 4447 (1984).
[8] K. Ohno and Y. Harada, in *Theoretical Models of Chemical Bonding, Part 3*, edited by Z. B. Macsić (Springer, Berlin, 1991), pp. 199–234.
[9] A. O. Bagawan, R. Muller-Fiedler, C. E. Brion, E. R. Davidson, and C. Boyle, Chem. Phys. **120**, 335 (1988).
[10] S. X. Tian, X. J. Chen, C. K. Xu, K. Z. Xu, L. F. Yuan, and J. L. Yang, J. Electron Spectrosc. Relat. Phenom. **105**, 99 (1999).
[11] P. E. Siska, Rev. Mod. Phys. **65**, 337 (1993).
[12] E. Illenberger and A. Niehaus, Z. Phys. B **20**, 3590 (1975).
[13] A. Pesnelle, G. Watel, and C. Manus, J. Chem. Phys. **62**, 350 (1975).
[14] W. Lee and R. Martin, J. Chem. Phys. **63**, 962 (1975).
[15] T. Parr and R. Martin, J. Chem. Phys. **69**, 1613 (1978).
[16] M. R. Woodard, R. C. Sharp, M. Seely, and E. E. Muschlitz, Jr., J. Chem. Phys. **69**, 2978 (1978).
[17] T. P. Parr, D. M. Parr, and R. M. Martin, J. Chem. Phys. **76**, 316 (1982).
[18] L. Appolloni, B. Brunetti, J. Hermanussen, F. Vecchiocattivi, and G. G. Volpi, J. Chem. Phys. **87**, 3804 (1987).
[19] K. Ohno, T. Takami, K. Mitsuke, and T. Ishida, J. Chem. Phys. **94**, 2675 (1991).
[20] K. Mitsuke, T. Takami, and K. Ohno, J. Chem. Phys. **91**, 1618 (1989).
[21] T. Takami, K. Mitsuke, and K. Ohno, J. Chem. Phys. **95**, 918 (1991).
[22] K. Ohno, H. Yamakado, T. Ogawa, and T. Yamata, J. Chem. Phys. **105**, 7536 (1996).
[23] T. Takami and K. Ohno, J. Chem. Phys. **96**, 6523 (1992).
[24] D. C. Dunlavy, D. W. Martin, and P. E. Siska, J. Chem. Phys. **93**, 5347 (1990).
[25] D. C. Dunlavy and P. E. Siska, J. Phys. Chem. **100**, 21 (1996).
[26] E. J. Longley, D. C. Dunlavy, M. F. Falcetta, H. M. Bevsek, and P. E. Siska, J. Phys. Chem. **97**, 2097 (1993).
[27] H. Nakamura, J. Phys. Soc. Jpn. **26**, 1473 (1969).
[28] W. H. Miller, J. Chem. Phys. **52**, 3563 (1970).
[29] W. H. Miller, C. A. Slocomb, and H. F. Schaefer III, J. Chem. Phys. **56**, 1347 (1972).
[30] A. P. Hickman and H. Morgner, J. Chem. Phys. **67**, 5484 (1977).
[31] M. Kimura and N. F. Lane, Phys. Rev. A **41**, 5938 (1990).
[32] M. Movre and W. Meyer, J. Chem. Phys. **106**, 7139 (1997).
[33] M. Movre, L. Thiel, and W. Meyer, J. Chem. Phys. **113**, 1484 (2000).
[34] B. J. Garrison, W. H. Miller, and H. F. Schaefer, J. Chem. Phys. **59**, 3193 (1973).
[35] A. Merz, M. W. Müller, M.-W. Ruf, H. Hotop, W. Mayer, and M. Movre, Chem. Phys. **145**, 219 (1990).
[36] J. C. Bellum and D. A. Micha, Phys. Rev. A **18**, 1435 (1978).
[37] T. Ishida and H. Katagiri, J. Phys. Chem. A **105**, 9379 (2001).
[38] J. S. Cohen and N. F. Lane, J. Chem. Phys. **66**, 586 (1977).
[39] T. Ishida, Chem. Phys. Lett. **191**, 1 (1992).
[40] T. Ishida, Chem. Phys. Lett. **211**, 1 (1993).
[41] T. Ishida and K. Horime, J. Chem. Phys. **105**, 5380 (1996).
[42] T. Ogawa and K. Ohno, J. Chem. Phys. **110**, 3773 (1999).
[43] T. Ogawa and K. Ohno, J. Phys. Chem. A **103**, 9925 (1999).
[44] K. Ohno, M. Yamazaki, N. Kishimoto, T. Ogawa, and K. Takeshita, Chem. Phys. Lett. **332**, 167 (2000).
[45] M. Yamazaki, N. Kishimoto, M. Kurita, T. Ogawa, K. Ohno, and K. Takeshita, J. Electron Spectrosc. Relat. Phenom. **114–116**, 175 (2001).
[46] B. Haug, H. Morgner, and V. Staemmler, J. Phys. B **18**, 259 (1985).
[47] T. Ishida, J. Chem. Phys. **102**, 4169 (1995).
[48] H. Feshbach, Ann. Phys. (N.Y.) **5**, 357 (1958); **19**, 287 (1962).
[49] A. P. Hickman, A. D. Isaacson, and W. H. Miller, J. Chem. Phys. **66**, 1492 (1977).
[50] E. W. Rothe, R. H. Neynaber, and S. Trujillo, J. Chem. Phys. **42**, 3310 (1965).
[51] H. Hotop, Radiat. Res. **59**, 379 (1974).
[52] H. Haberland, Y. T. Lee, and P. E. Siska, Adv. Chem. Phys. **45**, 487 (1981).
[53] H. Hotop, T. E. Roth, M.-W. Ruf, and A. J. Yencha, Theor. Chem. Acc. **100**, 36 (1998).
[54] P. H. Kasai, J. Am. Chem. Soc. **120**, 7884 (1998).
[55] K. Ohshimo, H. Tsunoyama, Y. Yamakita, F. Misaizu, and K. Ohno, Chem. Phys. Lett. **301**, 356 (1999).
[56] I. Tokue, Y. Sakai, and K. Yamasaki, J. Chem. Phys. **106**, 4491 (1997).
[57] B. Brunetti, P. Candori, J. De Andres, F. Pirani, M. Rosi, S. Falcinelli, and F. Vecchiocattivi, J. Phys. Chem. A **101**, 7505 (1997).
[58] M. Yamato, H. Ohoyama, and T. Kasai, J. Phys. Chem. A **105**, 2967 (2001).
[59] M. Yamazaki, S. Maeda, N. Kishimoto, and K. Ohno, Chem. Phys. Lett. **355**, 311 (2002).
[60] A. Berning and H.-J. Werner, J. Chem. Phys. **100**, 1953 (1994).
[61] J. V. Ortiz, J. Chem. Phys. **104**, 7599 (1996).
[62] J. L. Gardner and J. A. R Samson, J. Electron Spectrosc. Relat. Phenom. **8**, 469 (1976).
[63] K. Kimura, S. Katsumata, Y. Achiba, T. Yamazaki, and S. Iwata, *Handbook of He I Photoelectron Spectra of Fundamental Organic Molecules* (Japan Scientific, Tokyo, 1981).
[64] M. J. Frisch, G. W. Trucks, H. B. Schlegel *et al.*, GAUSSIAN 94, Revision C.3, Gaussian, Inc. Pittsburgh, PA, 1995.
[65] S. F. Boys and F. Bernardi, Mol. Phys. **19**, 553 (1970).
[66] T. Pasinszki, H. Yamakado, and K. Ohno, J. Phys. Chem. **99**, 14678 (1995).
[67] H. Yamakado, M. Yamauchi, S. Hoshino, and K. Ohno, J. Phys. Chem. **99**, 17093 (1995).
[68] H. Yamakado, T. Ogawa, and K. Ohno, J. Phys. Chem. A **101**, 3887 (1997).
[69] N. Kishimoto, J. Aizawa, H. Yamakado, and K. Ohno, J. Phys. Chem. A **101**, 5038 (1997).
[70] M. Yamauchi, H. Yamakado, and K. Ohno, J. Phys. Chem. A **101**, 6184 (1997).
[71] T. Pasinszki, N. Kishimoto, and K. Ohno, J. Phys. Chem. A **103**, 6746 (1999).
[72] N. Kishimoto and K. Ohno, J. Phys. Chem. A **104**, 6940 (2000).
[73] W. H. Miller and H. Morgner, J. Chem. Phys. **67**, 4923 (1977).
[74] R. S. Mulliken, J. Chim. Phys. **46**, 497 (1949).
[75] Vu. N. Demikov, Sov. Phys. JETP **18**, 138 (1964).
[76] S.-I. Choi, J. Jortner, S. A. Rice, and R. Silbey, J. Chem. Phys. **41**, 3294 (1964).
[77] R. E. Olson, F. T. Smith, and E. Bauer, Appl. Opt. **10**, 1848 (1971).
[78] R. E. Olson, Phys. Rev. **6**, 1031 (1972).
[79] D. J. Evans, Mol. Phys. **34**, 317 (1977).
[80] D. J. Evans and S. Murad, Mol. Phys. **34**, 327 (1977).
[81] T. H. Lee and J. W. Rabalais, J. Chem. Phys. **61**, 2747 (1974).

[82] M. Gochel-Dupuis, J. Delwiche, M.-J. Hubin-Franskin, and J. E. Collin, Chem. Phys. Lett. **193**, 41 (1992).
[83] A. D. Isaacson, A. P. Hickman, and W. H. Miller, J. Chem. Phys. **67**, 370 (1977).
[84] P. E. Siska, Chem. Phys. Lett. **63**, 25 (1979).
[85] P. E. Siska, J. Chem. Phys. **71**, 3942 (1979).
[86] D. W. Martin and P. E. Siska, J. Chem. Phys. **82**, 2630 (1985).
[87] K. Ohno and S. Sunada, Proc. Indian Acad. Sci. (Chem. Sci) **106**, 327 (1994).
[88] S. Hoshino and K. Ohno, J. Am. Chem. Soc. **119**, 8276 (1997).
[89] J. Katriel and E. R. Davidson, Proc. Natl. Acad. Sci. U.S.A. **77**, 4403 (1980).
[90] M. Albertí, J. M. Lucas, B. Brunetti, F. Pirani, M. Stramaccia, M. Rosi, and F. Vecchiocattivi, J. Phys. Chem. A **104**, 1405 (2000).